Supplementary Information for

Mucinase-engineered cell membrane nanovesicles degrade the glycocalyx shield to potentiate antitumor immunity

Xiaorui Geng[a,1], Silan Liu[a,b,c,1], Yuanwei Pan[a], Yun Ge[a,b,d,2], and Lang Rao[a,b,2]

[a] Institute of Chemical Biology, Shenzhen Bay Laboratory, Shenzhen 518132, China.
[b] Shenzhen Medical Academy of Research and Translation, Shenzhen 518107, China.
[c] Westlake University, Hangzhou 310030, China.
[d] State Key Laboratory of Chemical Oncogenomics, School of Chemical Biology and Biotechnology, Peking University Shenzhen Graduate School, Shenzhen 518055, China.
[1] X.G. and S.L. contributed equally to this work.
[2] Corresponding e-mail: geyun@szbl.ac.cn (Y.G.); lrao@szbl.ac.cn (L.R.).

This PDF file includes:

Supplementary Methods

Plasmid and subcloning

All StcE variants, each engineered with a secretion signal sequence, were generated using the pET30a plasmid as a template. SpyCatcher (SC) or StcE variants bearing an N-terminal HA tag were cloned into the pDisplay™ expression vector for cell surface display. Subsequently, constructs containing a signal peptide and the PDGFRβ transmembrane domain were subcloned into a lentiviral vector that co-expresses Green Fluorescent Protein (GFP) as a selection marker to facilitate the generation of stable cell lines.

Cell culture and transfection

HEK293T, CT26, 4T1, and RAW264.7 cells were maintained in Dulbecco's Modified Eagle Medium (DMEM) supplemented with 10% fetal bovine serum (FBS) and 1% penicillin–streptomycin. All cell lines were cultured in a humidified incubator at 37 °C with 5% CO_2. Transfections were performed using polyethylenimine (PEI) according to the manufacturer's protocol.

Protein expression and purification

Protein expression and purification were performed as previously described (1). Briefly, sequence-verified plasmids were transformed into Escherichia coli BL21 (DE3) cells, which were then cultured in sterile medium containing 30 μg/mL kanamycin. At an OD_{600} of 0.6, protein expression was induced with 0.3 mM IPTG, followed by overnight incubation. Bacteria were harvested by centrifugation (5,000 × g, 30 min, 4 °C). The resulting bacteria pellet was lysed by sonication, and the lysate was clarified by centrifugation (10,000 × g, 30 min, 4 °C). The supernatant, containing the crude protein, was loaded onto an AKTA purification system. Impurities were removed using a wash buffer (20 mM Tris-HCl pH 7.4, 150 mM NaCl, 40 mM imidazole), and the target protein was eluted with an elution buffer (20 mM Tris-HCl pH 7.4, 150 mM NaCl, 250 mM imidazole). The purified protein was changed into PBS buffer and stored at -80 °C.

Silver staining of StcE-treated C1INH

As previously reported (2), C1INH (Novoprotein) was treated with StcE variants at a 1:10 enzyme-to-substrate (E/S) mass ratio in 50 mM ammonium bicarbonate. The reaction was incubated at 37 °C for 3 h in a total volume of 15 μL. Reaction products (0.5 μg) were separated by SDS-PAGE (150 V, 1 h) and visualized using a Fast Silver Stain Kit (Beyotime) according to the manufacturer's protocol.

Fluorescent labeling of NVs and single-molecule localization microscopy imaging

Microscopy setup and imaging buffer preparation were performed as previously reported (3). Vesicles at appropriate concentrations were immobilized onto chambered slides via electrostatic adsorption. Briefly, coverglass (Thorlabs) was incubated with 0.1 mg/mL poly-L-lysine (Sigma) at 37 °C for 2 h to generate a positively charged surface. Subsequently, 50 μL of NVs (1 mg/mL) was added and allowed to adsorb for 1 h, followed by three washes with PBS. For immunostaining, anti-His monoclonal antibody (NovBio) and AF647-conjugated CD47 protein (Novoprotein) were diluted 1:200 in PBS, and 40 μL of the mixture was added to the sample and incubated at 4 °C overnight. After washing, samples were incubated with 40 μL CF680-conjugated secondary antibody (1:500 dilution) at room temperature for 1 h, followed by three washes with PBS. For ratiometric multicolor single-molecule localization microscopy (SMLM) imaging, the 642 nm laser power density was adjusted to ~1.0 kW/cm². For two-color NVs

imaging, 20,000 frames were acquired with an exposure time of 30 ms per frame, with continuous reactivation using a 405 nm laser.

In vitro biocompatibility of StcE-nCD47-FNVs

The biocompatibility of StcE and StcE-nCD47-FNVs (derived from HEK293T-StcE and CT26-nCD47 cells) was evaluated using hemolysis and cytotoxicity assays, followed by *in vivo* toxicity assessment. For the hemolysis assay, red blood cells (RBCs) were collected from the whole blood of healthy BALB/c mice and suspended in PBS. The RBCs suspension was incubated with various concentrations of StcE or StcE-nCD47-FNVs (10-1000 μg/mL) at 37 °C for 2 h. PBS and deionized water served as negative and positive controls, respectively. After incubation, the samples were centrifuged at 10,000 rpm for 2 min, and the absorbance of the supernatant was measured at 540 nm to determine hemoglobin release. The percentage of hemolysis was calculated using a standard equation. The cytotoxicity of StcE and StcE-nCD47-FNVs was assessed using the bEnd.3 murine brain endothelioma cell line. Cells were seeded into 96-well plates at a density of 8,000 cells per well. After 12 h, the culture medium was replaced with serum-free medium containing various concentrations of the test agents (0-50 μg/mL). Following a 6 h incubation, cell viability was quantified using a Cell Counting Kit-8 (CCK-8) assay according to the manufacturer's protocol.

In vivo dosing

Seven days after tumor inoculation, CT26 tumor-bearing mice were randomly assigned to four dose groups (n = 6) to receive intravenous injections of StcE-nCD47-FNVs at a concentration of 1 mg/mL. The four groups received doses of 0, 60, 120, and 180 μg per mouse. For safety assessment, serum samples were collected from three mice per group 24 h after injection. The remaining mice were monitored every other day for general health, body weight, and tumor growth following injection.

ELISA assay

For ELISA assay, tumor tissues of equivalent weight were excised from each treatment group of the CT26 tumor-bearing mice, snap-frozen in liquid nitrogen, and stored at -80°C. For analysis, frozen tissues were homogenized in ice-cold PBS containing a protease inhibitor cocktail. The homogenates were further lysed by sonication (5 min, 4°C) and then clarified by centrifugation (10,000 × g, 15 min, 4°C). The concentrations of IFN-γ, Interleukin-6 (IL-6), Interleukin-10 (IL-10), and TGF-β in the resulting supernatants were quantified using commercial ELISA kits according to the manufacturer's protocols.

Immunofluorescence for CT26 subcutaneous tumor model

Fresh CT26 tumor tissues were collected and embedded in OCT compound, followed by rapid freezing in liquid nitrogen. Frozen tissues were sectioned at 10 μm thickness and air-dried at room temperature for 10 min. Sections were washed twice with PBS (5 min each), fixed with 4% paraformaldehyde for 10 min, and washed twice more with PBS (5 min each). Sections were then blocked with 1% BSA and 2% FBS for 30 min at room temperature and incubated overnight at 4°C with StcE*-AF647. After incubation, sections were washed twice with PBS (5 min each), counterstained with DAPI, and washed twice more before imaging.

Data availability

The data that support the findings of this study are available from the corresponding author upon reasonable request.

Reference

1. K. Pedram *et al.*, Design of a mucin-selective protease for targeted degradation of cancer-associated mucins. *Nat. Biotechnol.* **42**, 597–607 (2024).
2. S. A. Malaker *et al.*, The mucin-selective protease StcE enables molecular and functional analysis of human cancer-associated mucins. *Proc. Natl. Acad. Sci. USA* **116**, 7278–7287 (2019).
3. Y. Han, S. Fan, Y. Xin, Y. Yin, Channel-linked multi-emitter fitting enables fast and accurate multi-channel single-molecule localization microscopy. *Opt. Express* **33**, 32798–32815 (2025).

Supplementary Tables

Table S1. Main reagents and materials

Reagents	Source	Identifier
Live/Dead-BV510	BD Pharmingen	564406
CD45-APC-CY7	BD Pharmingen	557659
CD3-FITC	BD Pharmingen	553061
CD4-BV650	Biolegend	100555
CD8-BV605	BD Pharmingen	563152
GranB-APC	Biolegend	372204
Foxp3-PE	BD Pharmingen	563101
CD11b-FITC	BD Pharmingen	553310
F4/80-APC-R700	BD Pharmingen	565787
CD86-BV650	BD Pharmingen	564200
CD206-AF647	Biolegend	141712
CD49b-PE	BD Pharmingen	558759
MUC1-PE	Biolegend	355604
HA-pacific blue	Biolegend	901526
eBioscience™ cell proliferation Dye eFlourTM 670	Invitrogen	65-0840-85
His-APC	Biolegend	362605
CD47-PE	Biolegend	127508
anti-HA Rb	CST	3724
anti-His Ms	Proteintech	66005
anti-GAPDH Rb	HUABIO	ET1601-4
CFSE	Invitrogen	C34554

Table S2. List of main abbreviations

Abbreviation	Description
StcE	Secreted protease of C1 esterase inhibitor
StcE*	E447D mutant, lacking enzymatic activity
C1INH	C1 esterase inhibitor
AF647	Alexa Fluor 647
SC	SpyCatcher003
ST	SpyTag003
NVs	Derived from HEK293T /CT26/4T1 cells, no functional proteins
StcE- NVs	Derived from HEK293T-StcE cells, glycocalyx hydrolysis only
nCD47-NVs	Derived from CT26/4T1-nCD47 cells, CD47 blockade only
FNVs	HEK293T-NVs and NVs were fused at 1:3 mass ratio, no functional proteins
StcE-FNVs	StcE-NVs and NVs were fused at 1:3 mass ratio, glycocalyx hydrolysis only
nCD47-FNVs	HEK293T-NVs and nCD47-NVs were fused at 1:3 mass ratio, CD47 blockade only
StcE-nCD47-FNVs	StcE-NVs and nCD47-NVs were fused at 1:3 mass ratio, combination of glycocalyx hydrolysis and CD47 blockade
StcE*-nCD47-FNVs	StcE*-NVs and nCD47-NVs were fused at 1:3 mass ratio, combination of glycocalyx hydrolysis and CD47 blockade

Table. S3. Primers for qRT-PCR

Primer	Sequence
IFN-γ. *F*	CAGCAACAGCAAGGCGAAAAAGG
IFN-γ. *R*	TTTCCGCTTCCTGAGGCTGGAT
TNF-α. *F*	GGTGCCTATGTCTCAGCCTCTT
TNF-α. *R*	GCCATAGAACTGATGAGAGGGAG
IL-1β. *F*	TGGACCTTCCAGGATGAGGACA
IL-1β. *R*	GTTCATCTCGGAGCCTGTAGTG
IL-10. *F*	CGGGAAGACAATAACTGCACCC
IL-10. *R*	CGGTTAGCAGTATGTTGTCCAGC
GAPDH. *F*	CATCACTGCCACCCAGAAGACTG
GAPDH. *R*	ATGCCAGTGAGCTTCCCGTTCAG
CD47. *F*	GGTGGGAAACTACACTTGCGAAG
CD47. *R*	CTCCTCGTAAGAACAGGCTGATC

Table. S4. Complete sequence for cDNAs

Surface display nCD47 Igκ leader HA tag nCD47 Myc tag PDGFRβ TM domain P2A Enhanced GFP	ATGGAGACAGACACACTCCTGCTATGGGTACTGCTGCTC TGGGTTCCAGGTTCCACTGGTGACTATCCATATGATGTT CCAGATTATGCTATGGCCCAGGTGCAGCTGGTGGAGAG CGGCGGCGGCCTGGTGGAGCCTGGCGGCAGCCTGAGG CTGAGCTGCGCCGCCAGCGGCATCATCTTCAAGATCAA CGACATGGGCTGGTACAGGCAGGCCCCTGGCAAGAGG AGGGAGTGGGTGGCCGCCAGCACCGGCGGCGACGAGG CCATCTACAGGGACAGCGTGAAGGACAGGTTCACCATC AGCAGGGACGCCAAGAACAGCGTGTTCCTGCAGATGAA CAGCCTGAAGCCTGAGGACACCGCCGTGTACTACTGCA CCGCCGTGATCAGCACCGACAGGGACGGCACCGAGTG GAGGAGGTACTGGGGCCAGGGCACCCAGGTGACCGTG AGCAGCAGGCTGCAGGTCGACGAACAAAAACTCATCTC AGAAGAGGATCTGAATGCTGTGGGCCAGGACACGCAGG AGGTCATCGTGGTGCCACACTCCTTGCCCTTTAAGGTGG TGGTGATCTCAGCCATCCTGGCCCTGGTGGTGCTCACC ATCATCTCCCTTATCATCCTCATCATGCTTTGGCAGAAGA AGCCACGTCACCACCACCACCACCACGGATCCGGCGCA ACAAACTTCTCTCTGCTGAAACAAGCCGGAGATGTCGAA GAGAATCCTGGACCGGTGAGCAAGGGCGAGGAGCTGTT CACCGGGGTGGTGCCCATCCTGGTCGAGCTGGACGGC GACGTAAACGGCCACAAGTTCAGCGTGTCTGGCGAGGG CGAGGGCGATGCCACCTACGGCAAGCTGACCCTGAAGT TCATCTGCACCACCGGCAAGCTGCCCGTGCCCTGGCCC ACCCTCGTGACCACCCTGACCTACGGCGTGCAGTGCTT CAGCCGCTACCCCGACCACATGAAGCAGCACGACTTCT TCAAGTCCGCCATGCCCGAAGGCTACGTCCAGGAGCGC ACCATCTTCTTCAAGGACGACGGCAACTACAAGACCCGC GCCGAGGTGAAGTTCGAGGGCGACACCCTGGTGAACCG CATCGAGCTGAAGGGCATCGACTTCAAGGAGGACGGCA ACATCCTGGGGCACAAGCTGGAGTACAACTACAACAGC CACAACGTCTATATCATGGCCGACAAGCAGAAGAACGG CATCAAGGCGAACTTCAAGATCCGCCACAACATCGAGGA CGGCAGCGTGCAGCTCGCCGACCACTACCAGCAGAACA CCCCCATCGGCGACGGCCCCGTGCTGCTGCCCGACAAC CACTACCTGAGCACCCAGTCCGCCCTGAGCAAAGACCC CAACGAGAAGCGCGATCACATGGTCCTGCTGGAGTTCG TGACCGCCGCCGGGATCACTCTCGGCATGGACGAGCTG TACAAGTAA

Surface display SpyCatcher Igκ leader HA tag SpyCatcher Myc tag PDGFRβ TM domain P2A Enhanced GFP	ATGGAGACAGACACACTCCTGCTATGGGTACTGCTGCTC TGGGTTCCAGGTTCCACTGGTGACTATCCATATGATGTT CCAGATTATGCTGGAAGCGGAGTGACCACACTGAGCGG CCTGAGCGGCGAGCAGGGCCCTTCTGGAGACATGACAA CAGAGGAGGACAGCGCCACACACATCAAGTTCAGCAAG AGAGATGAGGACGGCAGAGAGCTGGCCGGCGCCACAA TGGAGCTGAGGGACAGCTCCGGCAAGACCATCAGCACA TGGATCAGCGACGGCCACGTGAAGGATTTTTACCTGTAC CCTGGCAAGTACACATTCGTGGAGACAGCCGCCCCTGA CGGCTACGAGGTGGCCACACCCATCGAGTTTACAGTGA ACGAGGACGGCCAGGTGACAGTGGACGGCGAGGCCAC CGAGGGCGACGCTCATACAAGGCTGCAGGTCGACGAAC AAAAACTCATCTCAGAAGAGGATCTGAATGCTGTGGGCC AGGACACGCAGGAGGTCATCGTGGTGCCACACTCCTTG CCCTTTAAGGTGGTGGTGATCTCAGCCATCCTGGCCCTG GTGGTGCTCACCATCATCTCCCTTATCATCCTCATCATG CTTTGGCAGAAGAAGCCACGTCACCACCACCACCACCA CGGATCCGGCGCAACAAACTTCTCTCTGCTGAAACAAGC CGGAGATGTCGAAGAGAATCCTGGACCGGTGAGCAAGG GCGAGGAGCTGTTCACCGGGGTGGTGCCCATCCTGGTC GAGCTGGACGGCGACGTAAACGGCCACAAGTTCAGCGT GTCTGGCGAGGGCGAGGGCGATGCCACCTACGGCAAG CTGACCCTGAAGTTCATCTGCACCACCGGCAAGCTGCC CGTGCCCTGGCCCACCCTCGTGACCACCCTGACCTACG GCGTGCAGTGCTTCAGCCGCTACCCCGACCACATGAAG CAGCACGACTTCTTCAAGTCCGCCATGCCCGAAGGCTA CGTCCAGGAGCGCACCATCTTCTTCAAGGACGACGGCA ACTACAAGACCCGCGCCGAGGTGAAGTTCGAGGGCGAC ACCCTGGTGAACCGCATCGAGCTGAAGGGCATCGACTT CAAGGAGGACGGCAACATCCTGGGGCACAAGCTGGAGT ACAACTACAACAGCCACAACGTCTATATCATGGCCGACA AGCAGAAGAACGGCATCAAGGCGAACTTCAAGATCCGC CACAACATCGAGGACGGCAGCGTGCAGCTCGCCGACCA CTACCAGCAGAACACCCCCATCGGCGACGGCCCCGTGC TGCTGCCCGACAACCACTACCTGAGCACCCAGTCCGCC CTGAGCAAAGACCCCAACGAGAAGCGCGATCACATGGT CCTGCTGGAGTTCGTGACCGCCGCCGGGATCACTCTCG GCATGGACGAGCTGTACAAGTAA

StcE Δ35ΔC-SpyTag (StcE without signal peptide and C terminus) *StcE Δ35ΔC* <u>SpyTag (003)</u>	ATGGCCGACAACAACAGCGCCATCTACTTCAACACCAGC CAGCCCATCAACGACCTGCAGGGCAGCCTGGCCGCCGA GGTGAAGTTCGCCCAGAGCCAGATCCTGCCCGCCCACC CCAAGGAGGGCGACAGCCAGCCCCACCTGACCAGCCT GAGAAAGAGCCTGCTGCTGGTGAGACCCGTGAAGGCCG ACGACAAGACCCCCGTGCAGGTGGAGGCCAGAGACGA CAACAACAAGATCCTGGGCACCCTGACCCTGTACCCCC CCAGCAGCCTGCCCGACACCATCTACCACCTGGACGGC GTGCCCGAGGGCGGCATCGACTTCACCCCCCACAACGG CACCAAGAAGATCATCAACACCGTGGCCGAGGTGAACA AGCTGAGCGACGCCAGCGGCAGCAGCATCCACAGCCAC CTGACCAACAACGCCCTGGTGGAGATCCACACCGCCAA CGGCAGATGGGTGAGAGACATCTACCTGCCCCAGGGCC CCGACCTGGAGGGCAAGATGGTGAGATTCGTGAGCAGC GCCGGCTACAGCAGCACCGTGTTCTACGGCGACAGAAA GGTGACCCTGAGCGTGGGCAACACCCTGCTGTTCAAGT ACGTGAACGGCCAGTGGTTCAGAAGCGGCGAGCTGGAG AACAACAGAATCACCTACGCCCAGCACATCTGGAGCGC CGAGCTGCCCGCCCACTGGATCGTGCCCGGCCTGAACC TGGTGATCAAGCAGGGCAACCTGAGCGGCAGACTGAAC GACATCAAGATCGGCGCCCCCGGCGAGCTGCTGCTGCA CACCATCGACATCGGCATGCTGACCACCCCCAGAGACA GATTCGACTTCGCCAAGGACAAGGAGGCCCACAGAGAG TACTTCCAGACCATCCCCGTGAGCAGAATGATCGTGAAC AACTACGCCCCCCTGCACCTGAAGGAGGTGATGCTGCC CACCGGCGAGCTGCTGACCGACATGGACCCCGGCAAC GGCGGCTGGCACAGCGGCACCATGAGACAGAGAATCG GCAAGGAGCTGGTGAGCCACGGCATCGACAACGCCAAC TACGGCCTGAACAGCACCGCCGGCCTGGGCGAGAACA GCCACCCCTACGTGGTGGCCCAGCTGGCCGCCCACAAC AGCAGAGGCAACTACGCCAACGGCATCCAGGTGCACGG CGGCAGCGGCGGCGGCGGCATCGTGACCCTGGACAGC ACCCTGGGCAACGAGTTCAGCCACGAGGTGGGCCACAA CTACGGCCTGGGCCACTACGTGGACGGCTTCAAGGGCA GCGTGCACAGAAGCGCCGAGAACAACAACAGCACCTGG GGCTGGGACGGCGACAAGAAGAGATTCATCCCCAACTT CTACCCCAGCCAGACCAACGAGAAGAGCTGCCTGAACA ACCAGTGCCAGGAGCCCTTCGACGGCCACAAGTTCGGC TTCGACGCCATGGCCGGCGGCAGCCCCTTCAGCGCCG CCAACAGATTCACCATGTACACCCCCAACAGCAGCGCCA TCATCCAGAGATTCTTCGAGAACAAGGCCGTGTTCGACA GCAGAAGCAGCACCGGCTTCAGCAAGTGGAACGCCGAC ACCCAGGAGATGGAGCCCTACGAGCACACCATCGACAG AGCCGAGCAGATCACCGCCAGCGTGAACGAGCTGAGCG AGAGCAAGATGGCCGAGCTGATGGCCGAGTACGCCGTG GTGAAGGTGCACATGTGGAACGGCAACTGGACCAGAAA CATCTACATCCCCACCGCCAGCGCCGACAACAGAGGCA GCATCCTGACCATCAACCACGAGGCCGGCTACAACAGC

	TACCTGTTCATCAACGGCGACGAGAAGGTGGTGAGCCA GGGCTACAAGAAGAGCTTCGTGAGCGACGGCCAGTTCT GGAAGGAGAGAGACGTGGTGGACACCAGAGAGGCCAG AAAGCCCGAGCAGTTCGGCGTGCCCGTGACCACCCTGG TGGGCTACTACGACCCCGAGGGCACCCTGAGCAGCTAC ATCTACCCCGCCATGTACGGCGCCTACGGCTTCACCTAC AGCGACGACAGCCAGAACCTGAGCGACAACGACTGCCA GCTGCAGGTGGACACCAAGGAGGGCCAGCTGAGATTCA GACTGGCCAACCACAGAGCCAACAACACCGTGATGAAC AAGTTCCACATCAACGTGCCCACCGAGAGCCAGCCCAC CCAGGCCACCCTGGTGTGCAACAACAAGATCCTGGACA CCAAGAGCCTGACCCCCGCCCCCGAGGGCCTGACCTAC ACCGTGAACGGCCAGGCCCTGCCCGCCAAGCGCGGCG TGCCGCATATTGTGATGGTGGATGCGTATAAACGCTATA AAGGAGGTGGCGGCGGTTCGGGTGGAGGTGGATCACTT CCAGAGACGGGCGGACACCACCACCACCACCACTGA

Supplementary Figures

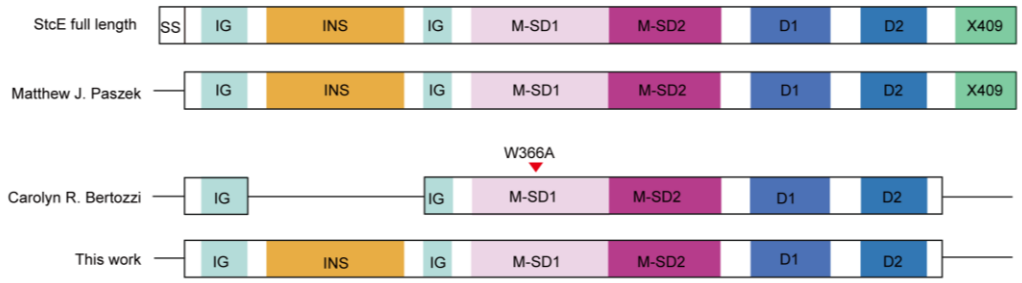

Fig. S1. Sequence comparison of representative StcE-based therapeutic constructs.

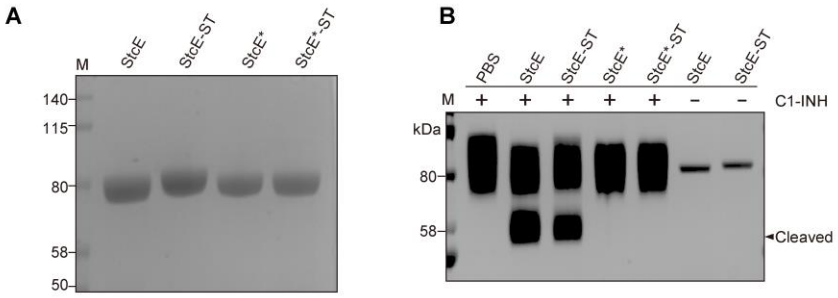

Fig. S2. Expression and enzymatic activity of StcE and StcE variants. (*A*) Coomassie blue staining of StcE, SpyTag-labeled StcE (StcE-ST), and ST-labeled inactive point mutant StcE* (StcE*-ST) (~80 kDa). (*B*) Mucinase activity assessed using C1-INH as substrate. Samples treated with StcE, StcE*, StcE-ST, or StcE*-ST (enzyme-to-substrate ratio 1:10) were visualized by silver staining. Cleaved products are indicated. StcE*: inactive mutant.

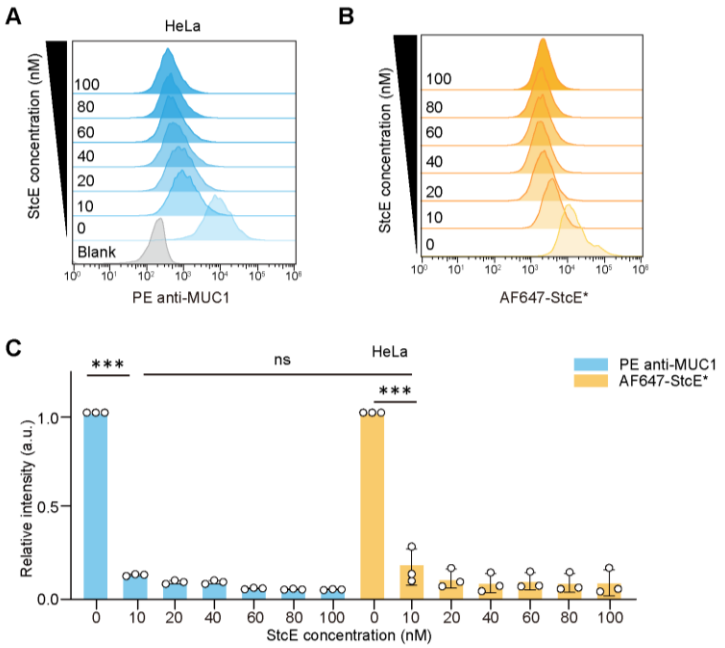

Fig. S3. StcE-mediated degradation of cell-surface mucins on HeLa cells. (*A-B*) Flow cytometry analysis of mucin levels after treatment with different StcE concentrations. (*C*) Normalized mucin intensity quantification using two staining reagents. Data are presented as mean ± S.D. (*n* = 3). StcE*: inactive mutant.

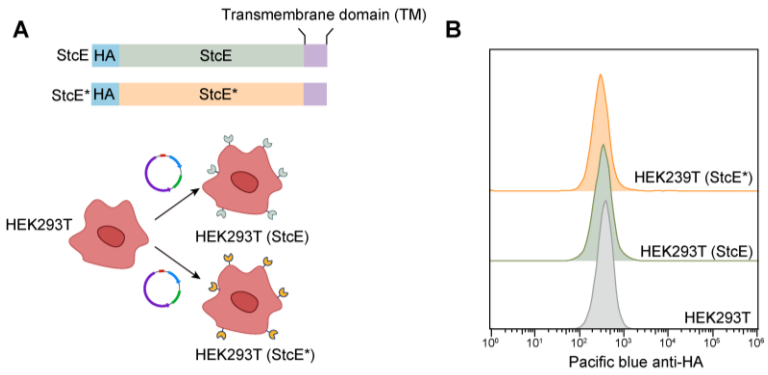

Fig. S4. Genetic display of StcE/StcE* on HEK293T cell surfaces. (*A*) Schematic of StcE display using pDisplay™-derived constructs with a transmembrane (TM) domain. (*B*) Flow cytometry of HA-tagged StcE/StcE* in engineered HEK293T stable transfected cells. StcE*: inactive mutant.

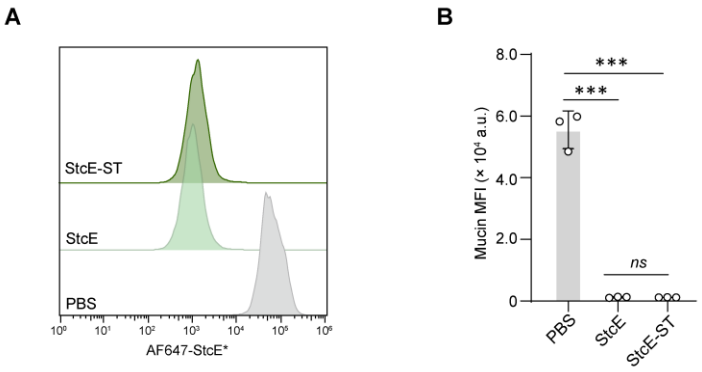

Fig. S5. Comparison of mucinase activity between StcE and ST-labeled StcE. (*A*) Flow cytometry analysis of HeLa cells-surface mucins after treatment. (*B*) Mean fluorescence intensity (MFI) quantification. Data are presented as mean ± S.D. (n = 3). StcE*: inactive mutant. *ns*: not significant; ***P < 0.001.

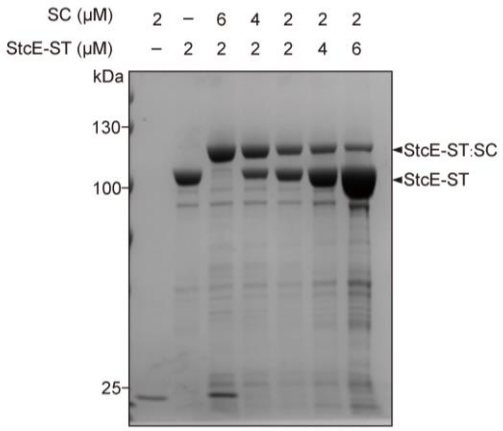

Fig. S6. *In vitro* bioconjugation of StcE-SpyTag (ST) with SpyCatcher (SC). SC was incubated with StcE-ST for 25 min, analyzed by SDS-PAGE with coomassie staining.

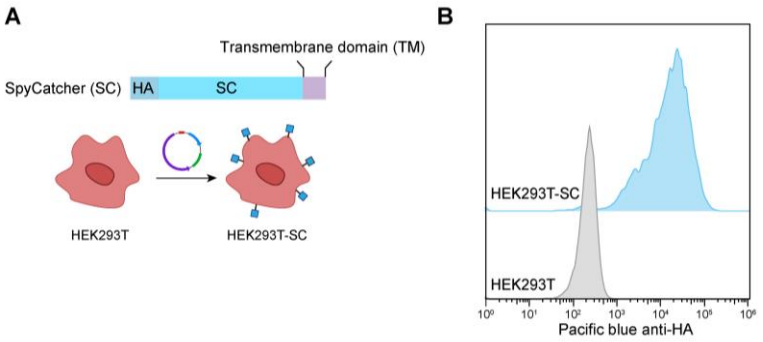

Fig. S7. SpyCatcher (SC) display on HEK293T cells. (*A*) Schematic of SC display using pDisplay™-derived constructs containing a TM domain. (*B*) Flow cytometry of HA-tagged SC on engineered HEK293T cells.

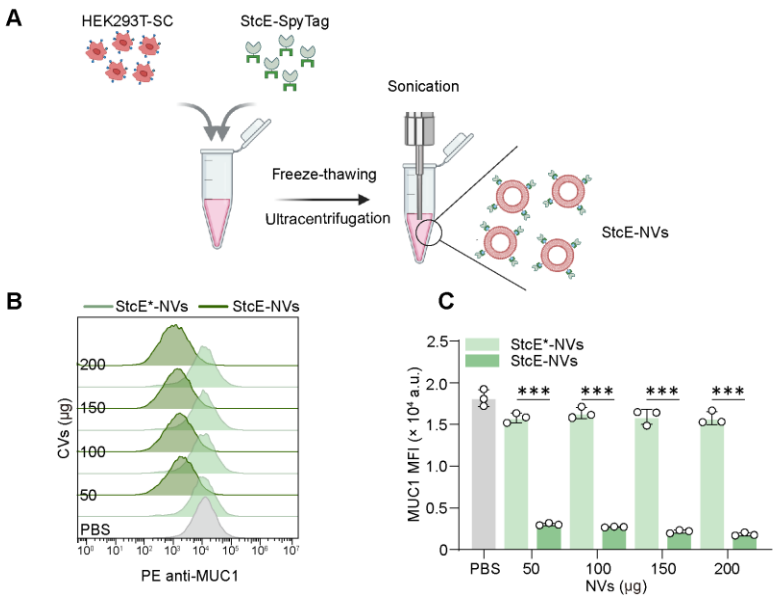

Fig. S8. Preparation and activity validation of StcE-NVs. (*A*) Schematic illustration of StcE-NVs preparation. (*B*) Flow cytometry analysis and (*C*) MFI quantification of MUC1 on HeLa cells after treatment with StcE-NVs, stained with PE-labelled anti-MUC1 antibody. Data are presented as mean ± S.D. (*n* = 3). StcE*: StcE inactive mutant.

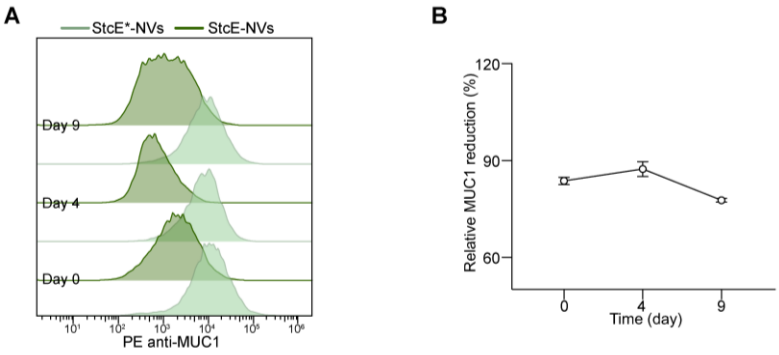

Fig. S9. Stability of StcE-NVs. (*A*) Flow cytometry analysis of MUC1 on HeLa cells after incubation with StcE-NVs or StcE*-NVs on day 0, 4, 9. (*B*) Change of the MUC1 protein level. Data are presented as mean ± S.D. (*n* = 3). StcE*: inactive mutant.

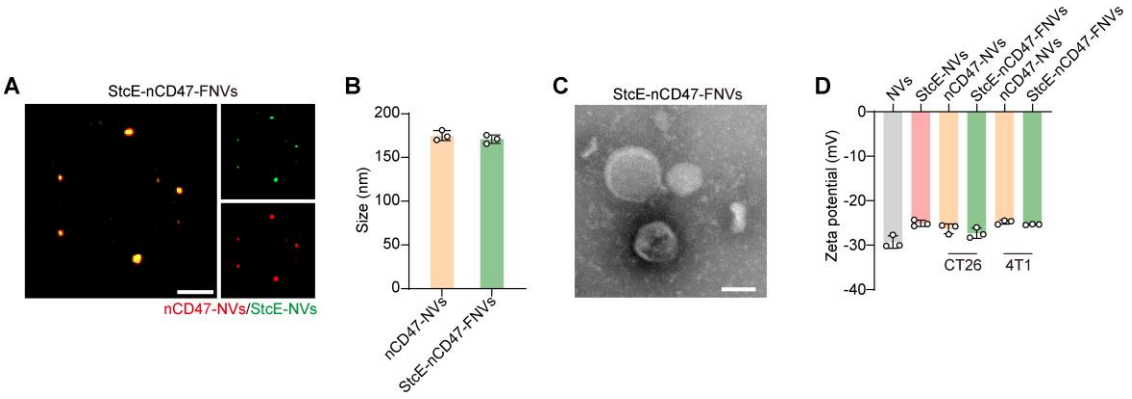

Fig. S10. Fusion of nCD47-NVs with StcE-NVs and characterization of 4T1-StcE-nCD47-FNVs. (*A*) CLSM images of fusion of DiI-labeled 4T1-nCD47-NVs (red) with DiO-labeled StcE-NVs (green). Scale bar, 5 μm. (*B*) Size distribution of 4T1-nCD47-NVs and 4T1-StcE-nCD47-FNVs. (*C*) TEM image of 4T1-StcE-nCD47-FNVs. Scale bar, 50 nm. (*D*) Zeta potential of HEK293T-NVs, StcE-NVs, CT26-nCD47-NVs, CT26-StcE-nCD47-FNVs, 4T1-nCD47-NVs, and 4T1-StcE-nCD47-FNVs. Data are presented as mean ± S.D. (*n* = 3).

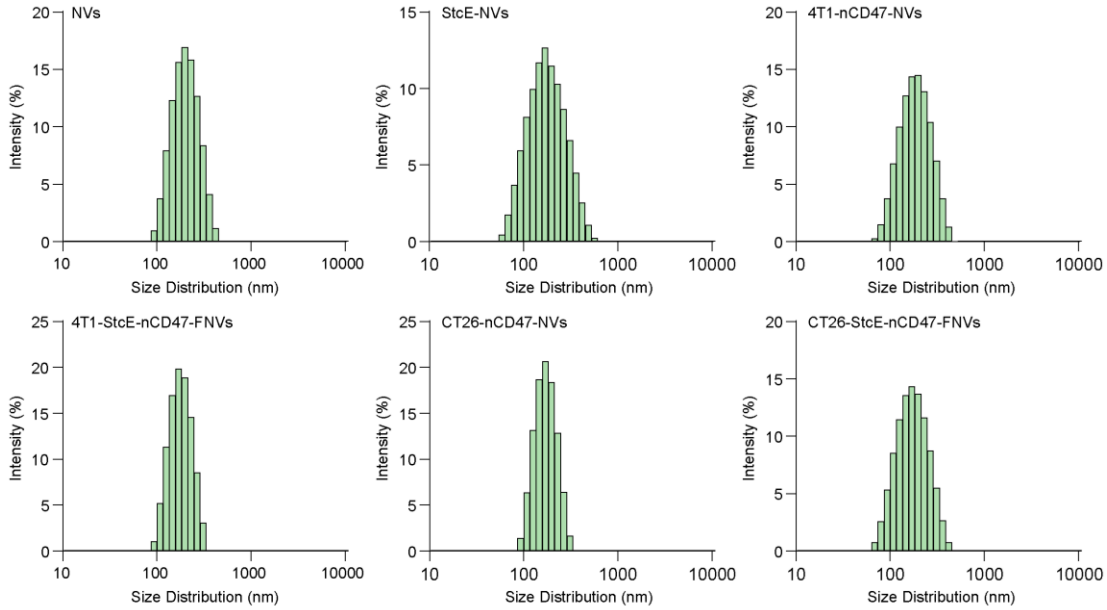

Fig. S11. Size distribution of different NVs.

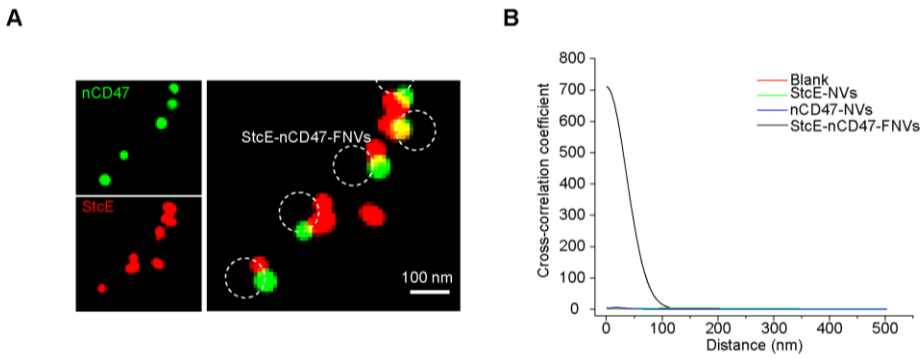

Fig. S12. The SMLM analyses of nCD47 and StcE on NVs. (A) Representative SMLM images showing the colocalization of nCD47 (green) and StcE (red) on StcE-nCD47-FNVs. White dashed circles (diameter = 100 nm) refer to a general size of NVs. (B) The cross-correlation coefficient analysis of different NVs as indicated.

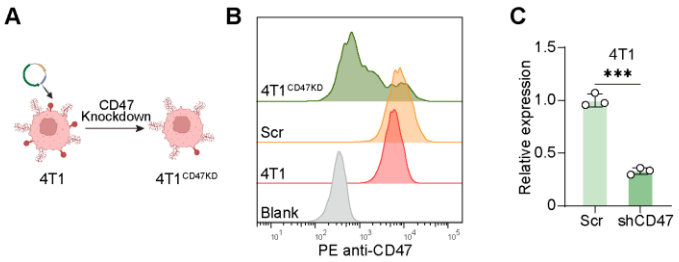

Fig. S13. CD47 knockdown in 4T1 cells. (*A*) Schematic of shRNA-mediated CD47 knockdown. (*B*) Flow cytometry of CD47 in 4T1 cells stably transfected with shScramble (Scr) or shCD47 RNA. (*C*) qPCR quantification of CD47 mRNA. (n = 3).

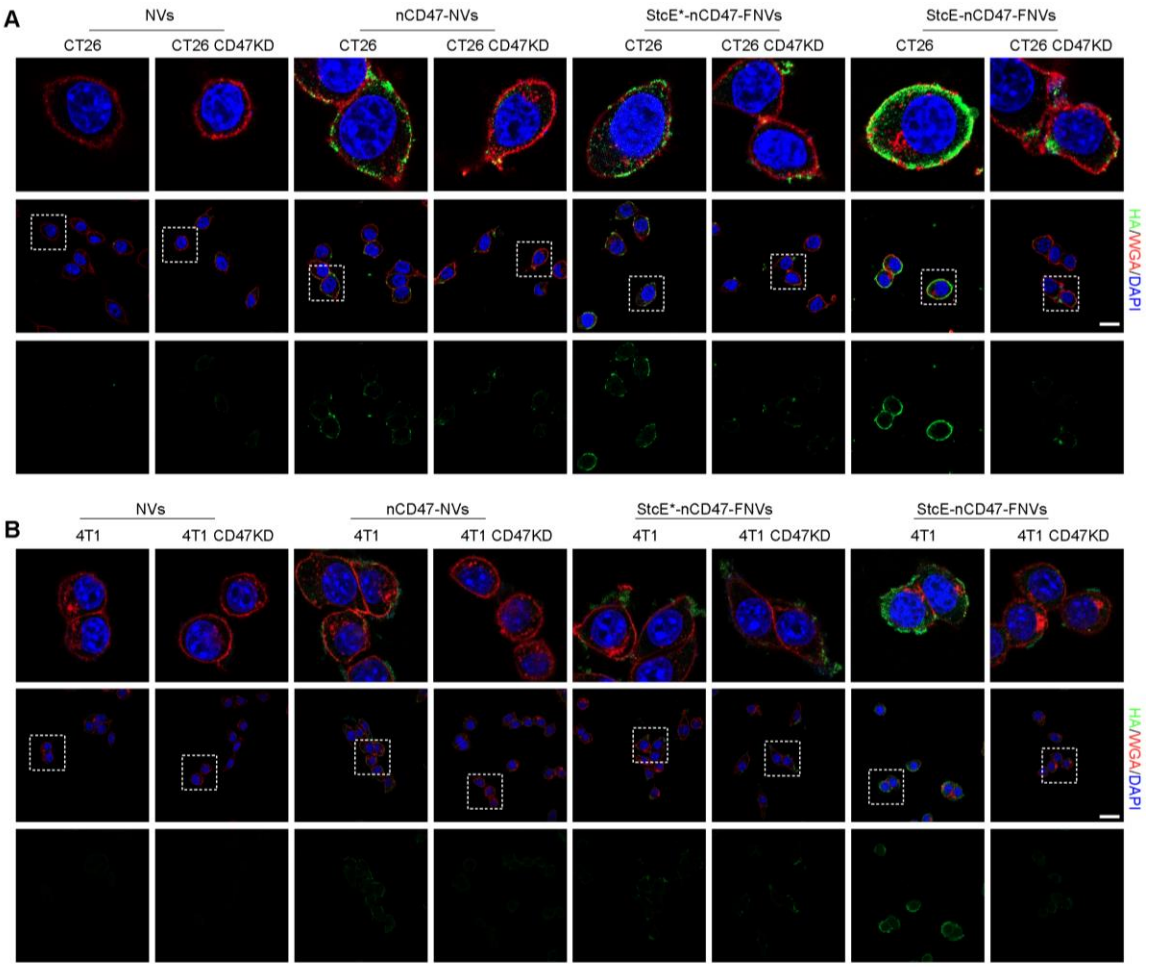

Fig. S14. Binding of nanovesicles to tumor cells is enhanced by CD47 targeting and StcE modification. (*A*) Confocal images of wild-type (WT) and CD47-knockdown (CD47KD) CT26 cells incubated with NVs, nCD47-NVs, StcE*-nCD47-FNVs, or StcE-nCD47-FNVs. Scale bar, 20 μm. (*B*) Confocal images of WT and CD47KD 4T1 cells incubated with NVs, nCD47-NVs, StcE*-nCD47-FNVs, or StcE-nCD47-FNVs. Scale bar, 20 μm.

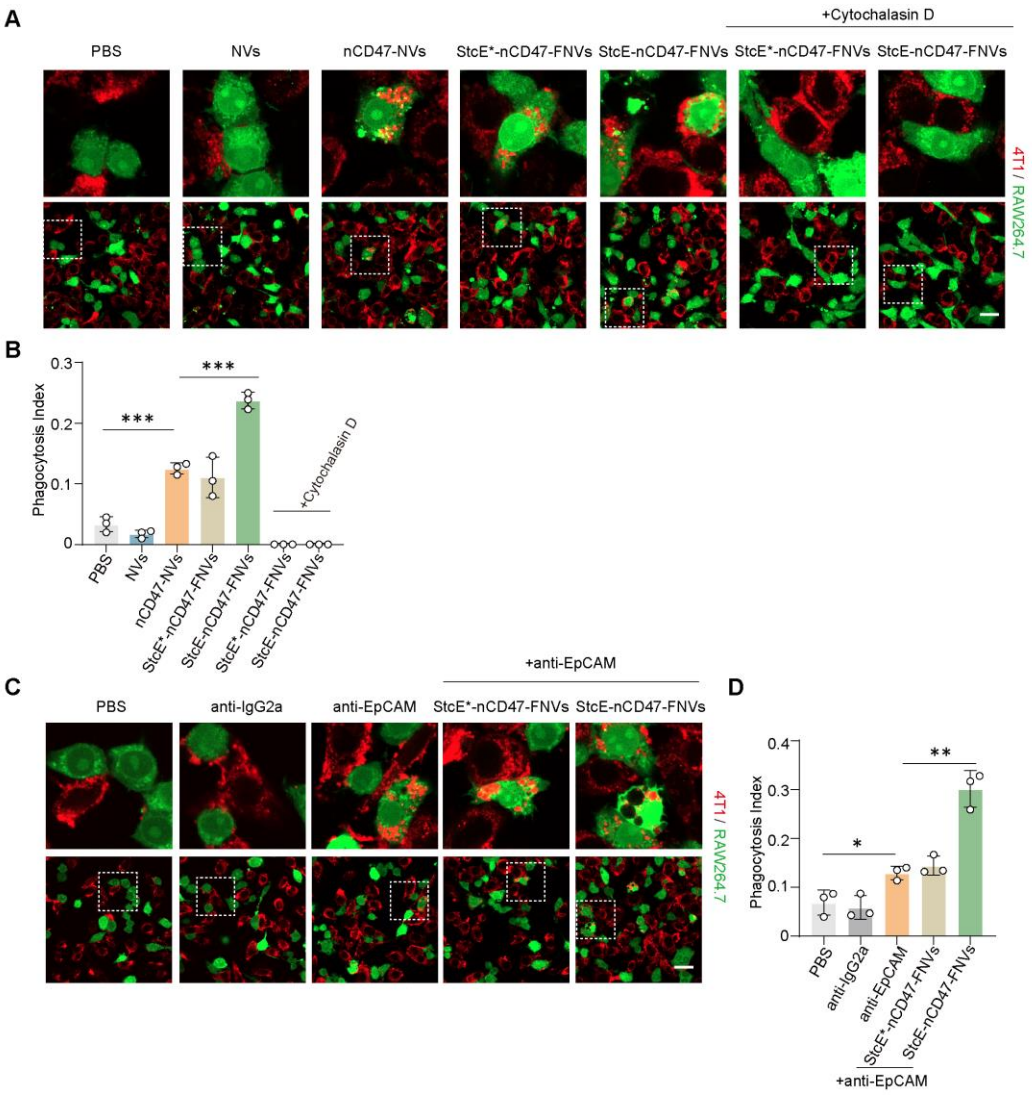

Fig. S15. CD47 blockade enhances macrophage-mediated phagocytosis *in vitro*. (*A*) Fluorescence images of phagocytosis assays induced by the indicated NVs. RAW264.7 macrophages were stained with CFSE (green), and 4T1 cells with eFluor670 (red). 1 μM Cytochalasin D was pretreated for 30 min at 37℃ prior to phagocytosis assay. Scale bar, 20 μm. (*B*) Quantification of the phagocytosis index of 4T1 cells by RAW264.7 macrophages. The phagocytosis index was calculated as the number of $CFSE^+$ tumor cells engulfed per 100 macrophages. (*C*) Fluorescence images of phagocytosis assays treated with opsonizing anti-EpCAM. RAW264.7 macrophages were stained with CFSE (green), and 4T1 cells with eFluor670 (red). Scale bar, 20 μm. (*D*) Quantification of the phagocytosis index of 4T1 cells by RAW264.7 macrophages. The phagocytosis index was calculated as the number of $CFSE^+$ tumor cells engulfed per 100 macrophages. Data are presented as mean ± S.D. (n = 3). *P < 0.05, **P < 0.01, ***P < 0.001. NVs and nCD47-NVs are from 4T1 and 4T1-nCD47 cells.

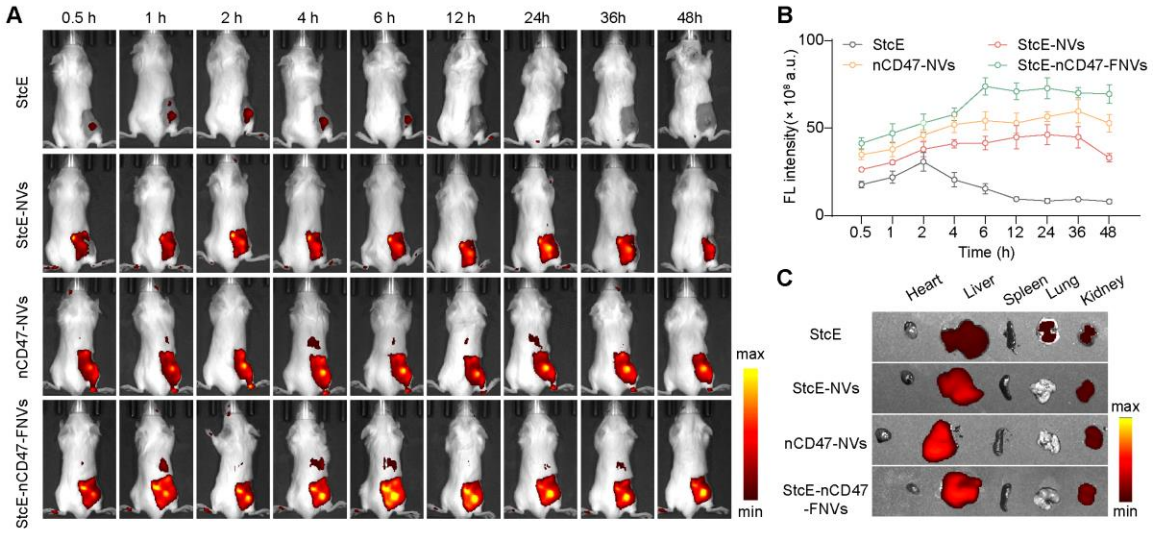

Fig. S16. *In vivo* biodistribution and tumor accumulation. (*A*) Representative *in vivo* fluorescence images (0.5 - 48 h) after Cy5.5-labeled StcE, StcE-NVs, CT26-nCD47-NVs, CT26-StcE-nCD47-FNVs injection. (*B*) Tumor fluorescence quantification, (n = 3). (*C*) Representative *ex vivo* fluorescence imaging of major organs.

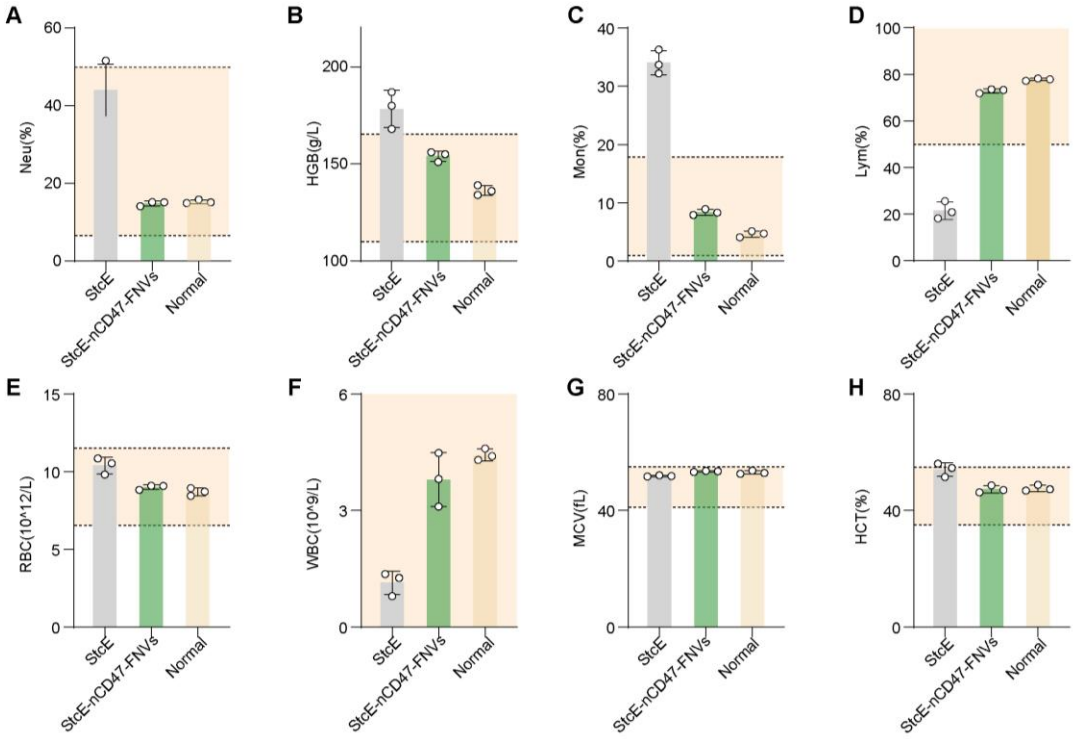

Fig. S17. Hematological analysis of CT26 tumor-bearing mice after intravenous injection of StcE, StcE-nCD47-FNVs. Parameters from a complete blood count (CBC) were measured, including: (*A*) neutrophils (Neu), (*B*) hemoglobin (HGB), (*C*) monocytes (Mon), (*D*) lymphocytes (Lym), (*E*) red blood cells (RBC), (*F*) white blood cells (WBC), (*G*) mean corpuscular volume (MCV), and (*H*)hematocrit (HCT). Safety ranges: orange shading, Data are presented as mean ± S.D. (*n* = 3). StcE-nCD47-FNVs (HEK293T-StcE-NVs: CT26-nCD47-NVs =1:3).

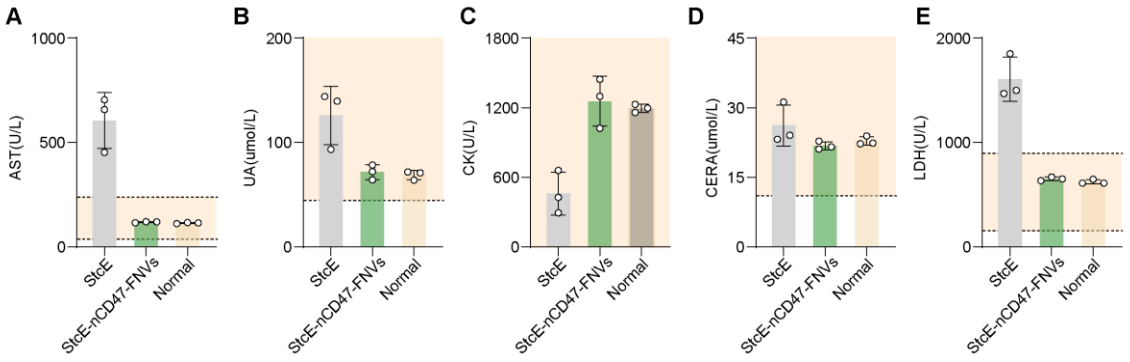

Fig. S18. Blood biochemistry analysis of CT26 tumor-bearing mice after StcE or StcE-nCD47-FNVs treatment. Serum levels of markers for liver function (*A*: AST), kidney function (*B*: UA, *D*: CREA), and general tissue or muscle damage (*C*: CK, *E*: LDH) were quantified. Safety ranges: orange shading. Data are presented as mean ± S.D. (*n* = 3). StcE-nCD47-FNVs (HEK293T-StcE-NVs: CT26-nCD47-NVs =1:3).

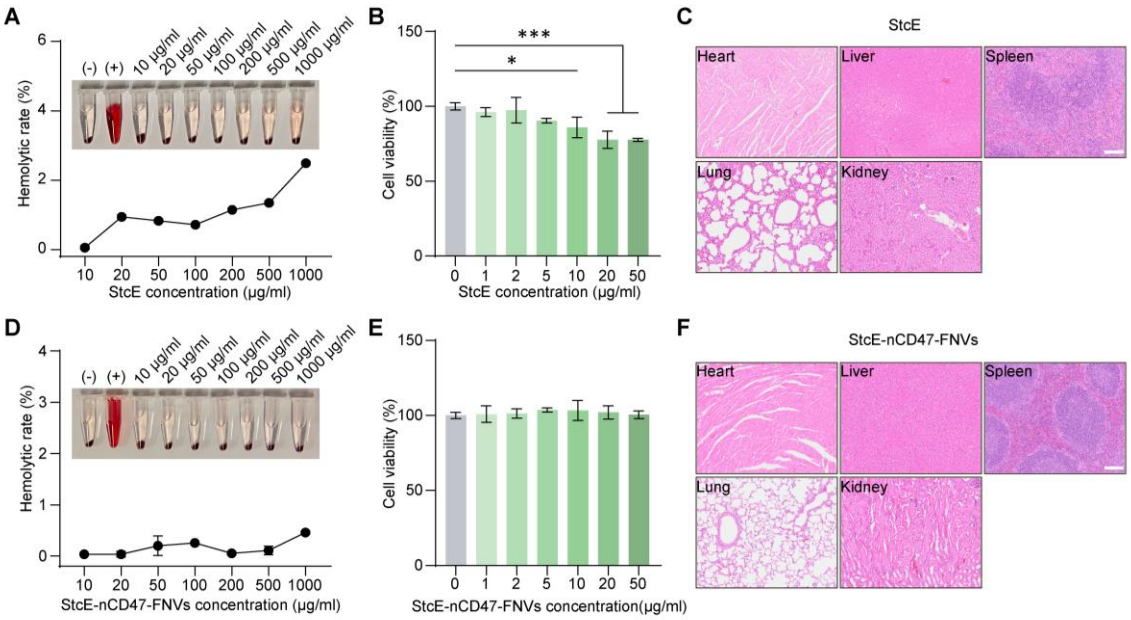

Fig. S19. Biocompatibility of StcE and StcE-nCD47-FNVs. (*A, D*) Red blood cell hemolysis. (*B, E*) bEnd.3 cell viability after 6 h incubation. (*C, F*) H&E-staining sections of major organs. Scale bars, 100 μm. StcE-nCD47-FNVs (HEK293T-StcE-NVs: CT26-nCD47-NVs =1:3). Data are presented as mean ± S.D. (*n* = 3). **P* < 0.05, ***P* < 0.01, ****P* < 0.001.

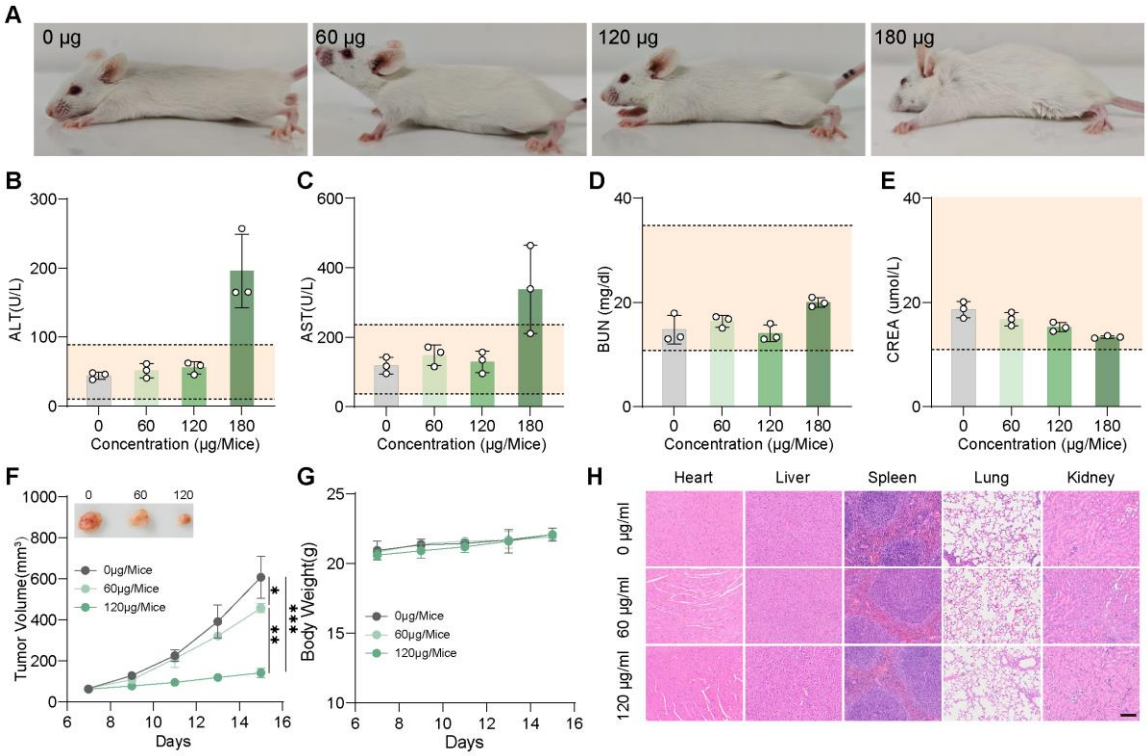

Fig. S20. Dose-escalation study of StcE-nCD47-FNVs in mice. (*A*) Representative photographs of mice 24 h after intravenous administration of StcE-nCD47-FNVs at doses of 0, 60, 120, and 180 μg per mouse. (*B-C*) Serum levels of ALT and AST in mice treated with different doses of StcE-nCD47-FNVs. The shaded area indicates the normal reference range for liver function markers. (*D-E*) Serum levels of blood BUN and CREA in mice treated with different doses of StcE-nCD47-FNVs. (*F*) Tumor growth curves of CT26 tumor-bearing mice. (*G*) Body weight changes of CT26 tumor-bearing mice. (*H*) H&E-stained sections of major organs from mice. Scale bar, 100 μm. Data are presented as mean ± S.D. (n = 3). *P < 0.05, **P < 0.01, ***P < 0.001.

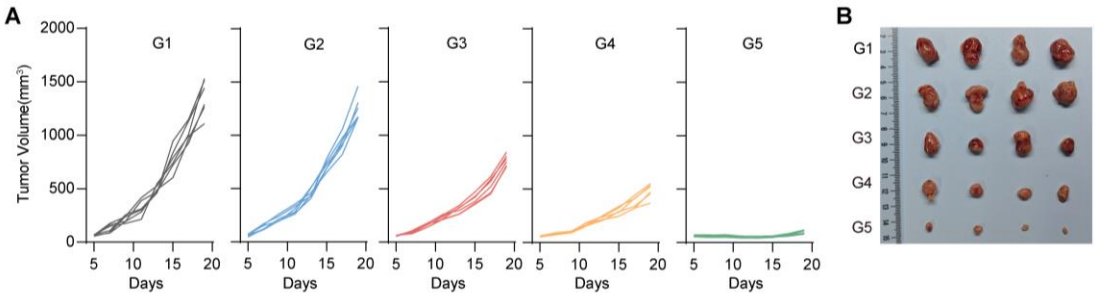

Fig. S21. *In vivo* anti-tumor efficacy of CT26 tumor-bearing mice. (*A*) Tumor growth curves of CT26 tumor-bearing mice received different treatments. (*B*) Representative images of tumors from all groups at the experimental endpoint. Related to Fig. 4.

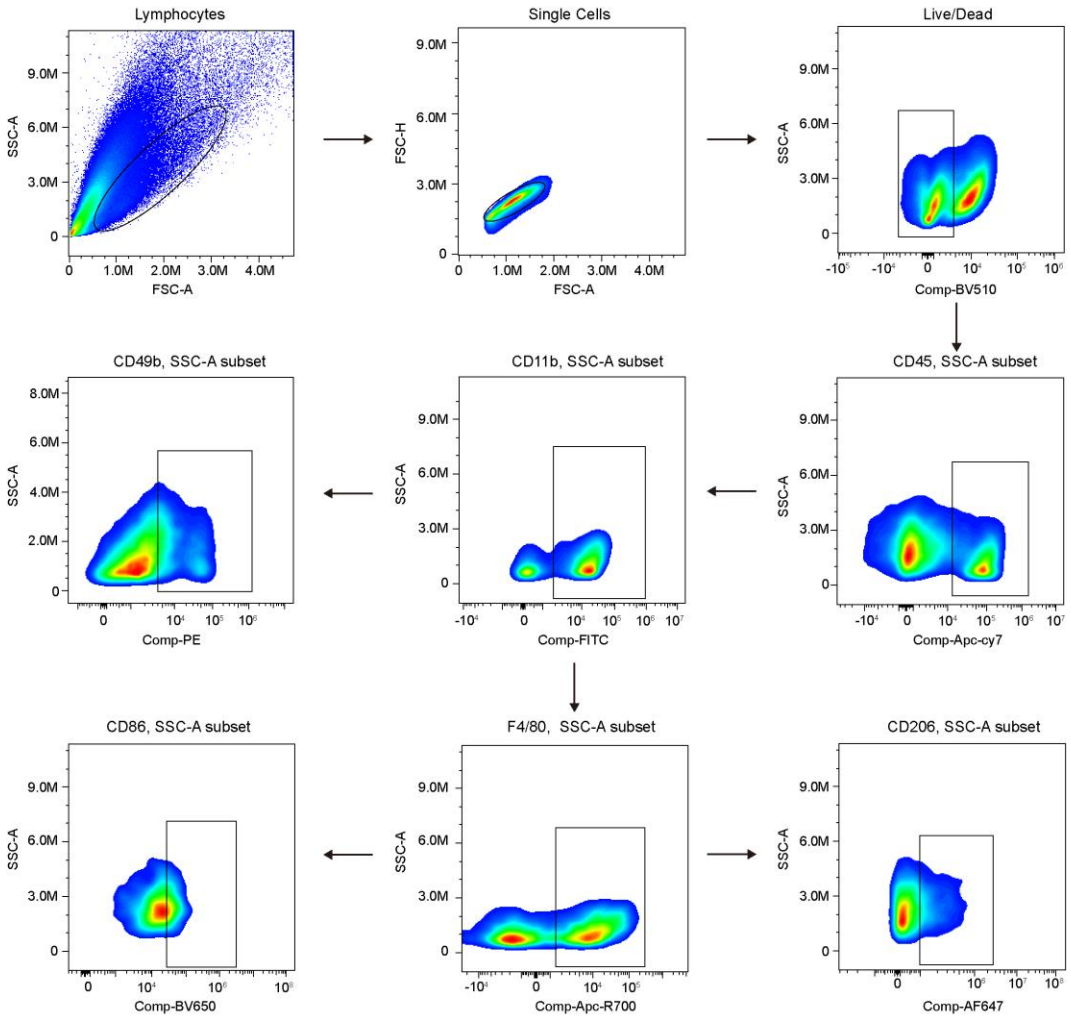

Fig. S22. Gating strategy for flow cytometry of macrophages and NK cells. Related to Fig. 4, S24, S26.

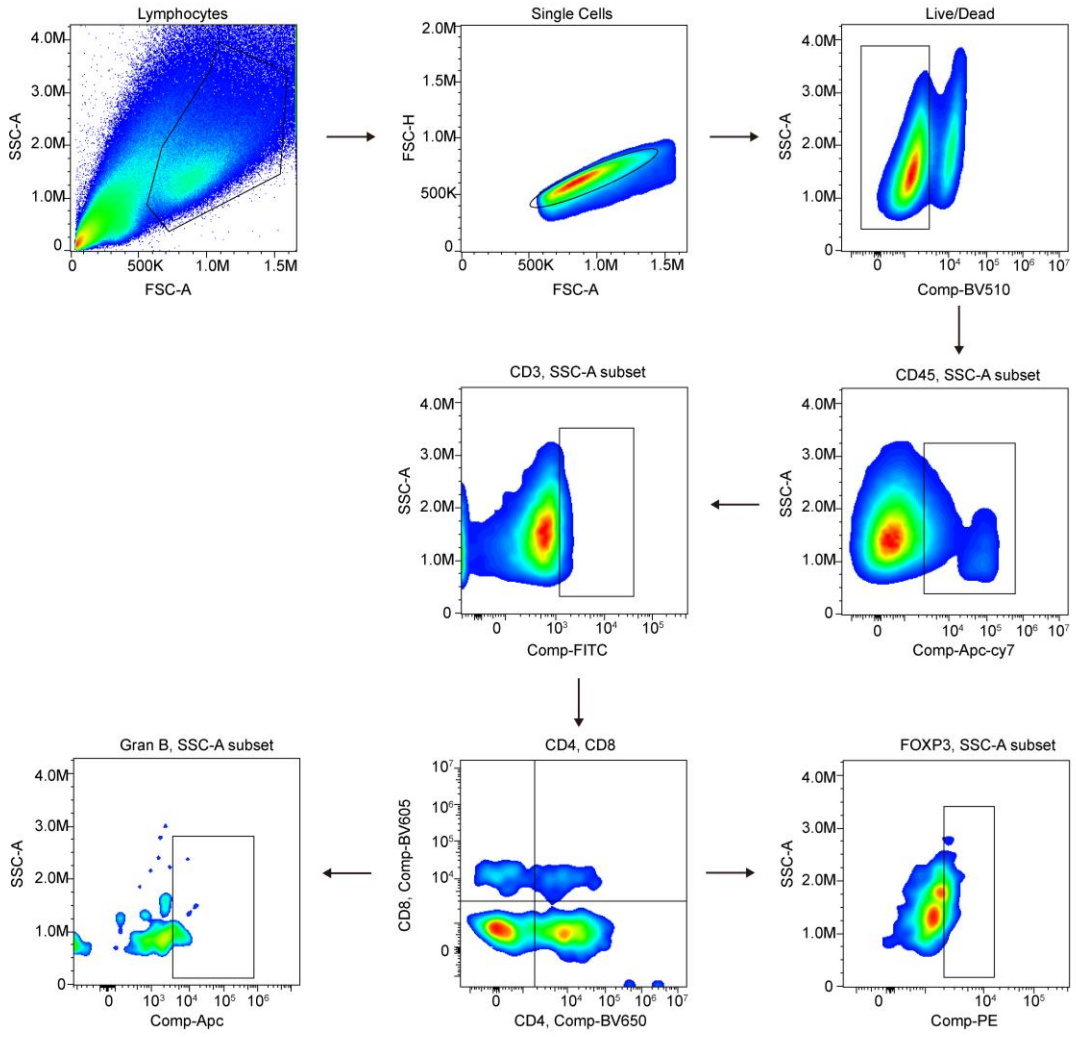

Fig. S23. Gating strategy for flow cytometry of tumor-infiltrating T cells. Related to Fig.4, S25, and S26.

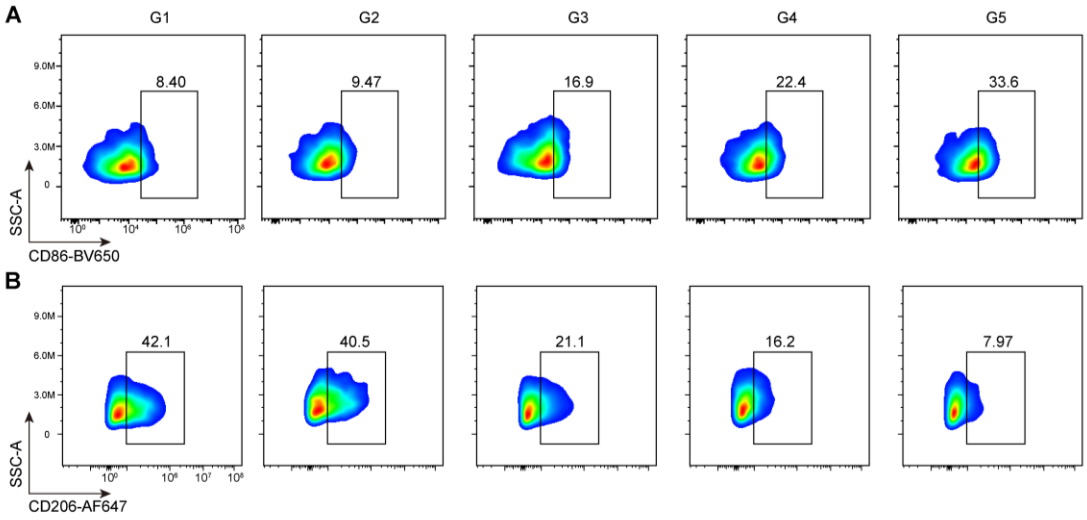

Fig. S24. Flow cytometry of tumor-infiltrating macrophage. (*A*) $CD86^+$ $CD206^-$ M1 phenotype macrophages within $CD11b^+$ $F4/80^+$ population. (*B*) $CD86^-$ $CD206^+$ M2 phenotype macrophages within $CD11b^+$ $F4/80^+$ population. Related to Fig. 4.

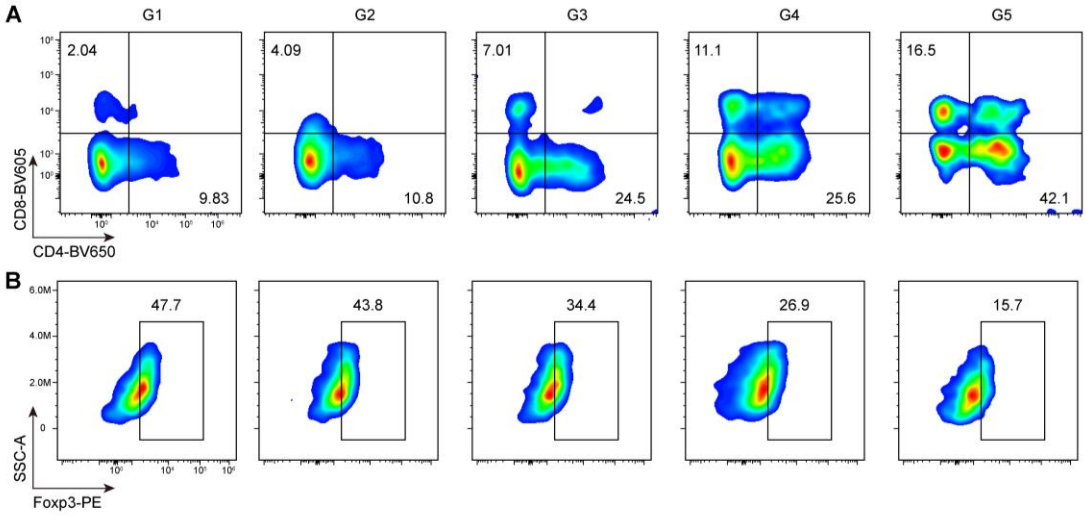

Fig. S25. Flow cytometry of tumor-infiltrating T cell. (*A*) $CD8^+$ cytotoxic T cells within $CD45^+$ $CD3^+$ lymphocytes. (*B*) $CD4^+$ $Foxp3^+$ regulatory T cells within $CD45^+$ $CD3^+$ lymphocytes. Related to Fig. 4.

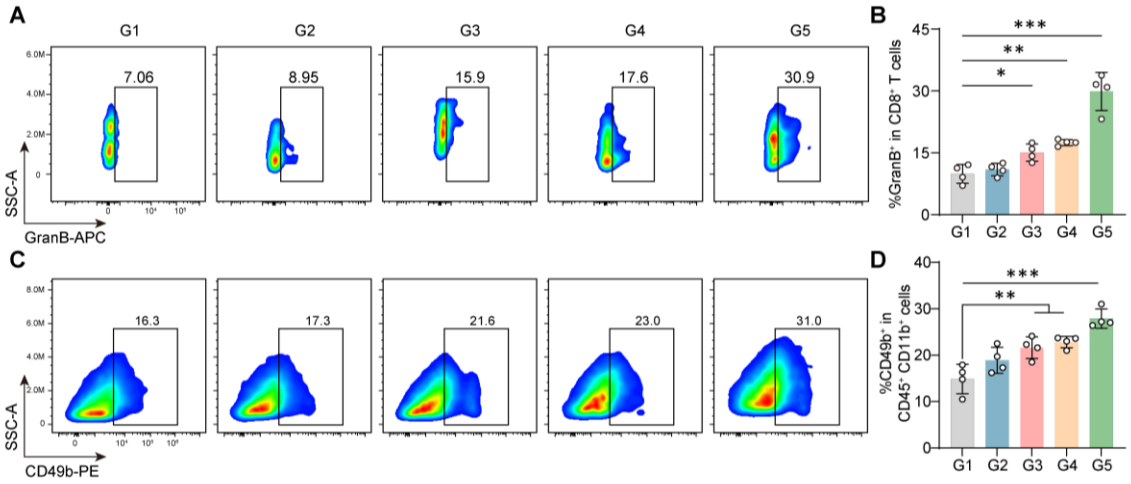

Fig. S26. Flow cytometry of cytotoxic CD8⁺ T cells and NK cell. (*A, B*) Flow cytometry plots and quantification of granzyme B⁺ cells in CD3⁺ CD8⁺ T cells. (*C, D*) Flow cytometry plots and quantification of CD49b⁺ NK cells in CD45⁺ CD11b⁺ population. Related to Fig. 4. Data are presented as mean ± S.D. (n = 4). *P < 0.05, **P < 0.01, ***P < 0.001.

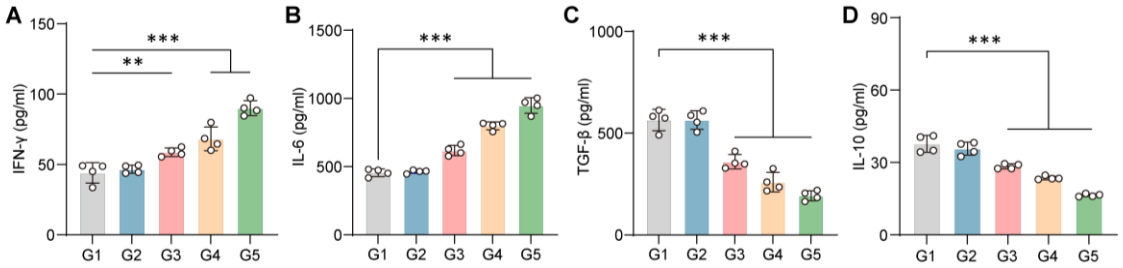

Fig. S27. Cytokine level in tumors. (*A*) IFN-γ levels in CT26 tumor. (*B*) IL-6 levels in CT26 tumor. (*C*) TGF-β levels in CT26 tumor. (*D*) IL-10 levels in CT26 tumor. Data are presented as mean ± S.D. (*n* = 4). ***P* < 0.01, ****P* < 0.001. Related to Fig. 4.

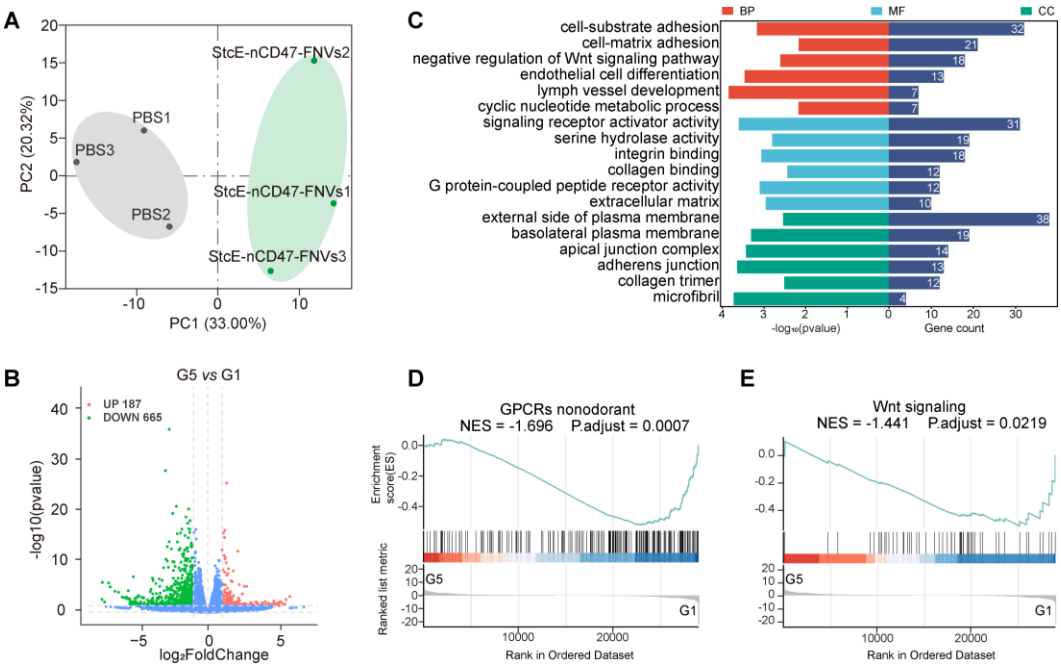

Fig. S28. RNA-sequencing analysis of tumor tissues from CT26 tumor-bearing mice after treatment. (*A*) Principal Component Analysis (PCA) plot of StcE-nCD47-FNVs group and PBS group. (*B*) Volcano plot of differentially expressed genes (DEGs) comparing StcE-nCD47-FNVs group with the PBS group. Upregulated and downregulated genes are indicated in red and green, respectively. (*C*) Gene Ontology (GO) analysis of DEGs between StcE-nCD47-FNVs group and PBS group. (*D, E*) Gene Set Enrichment Analysis (GSEA) of the "GPCRs nonodorant" (*D*) and "Wnt signaling" (*E*) pathways in G5 group. Related to Fig. 4.

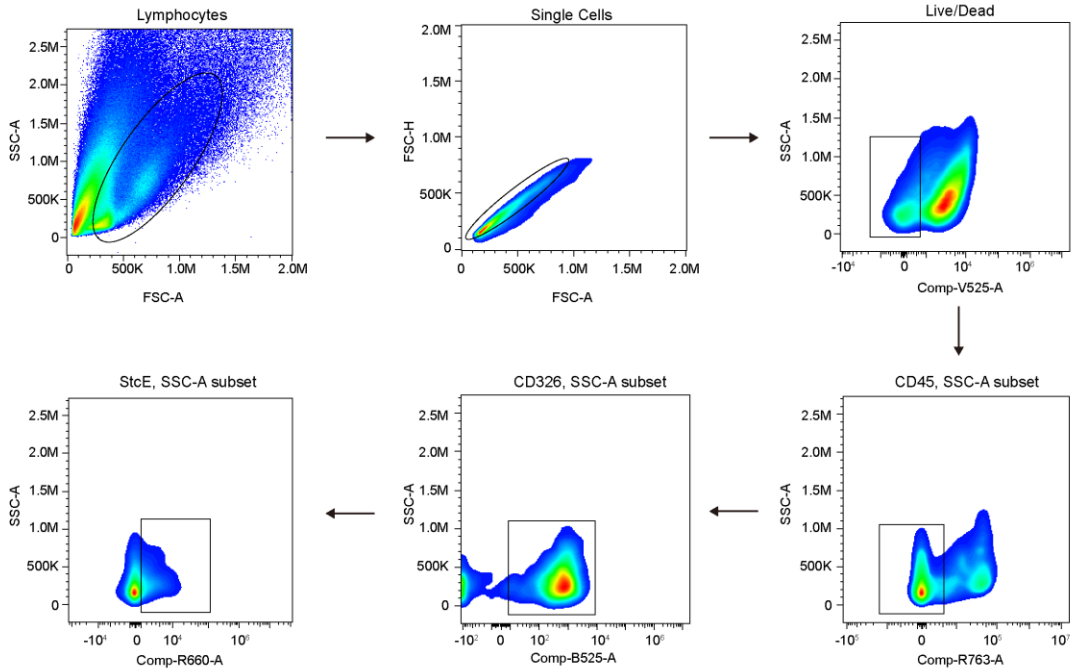

Fig. S29. Gating strategy for flow cytometry of mucin level on tumor cells. Related to Fig. S30.

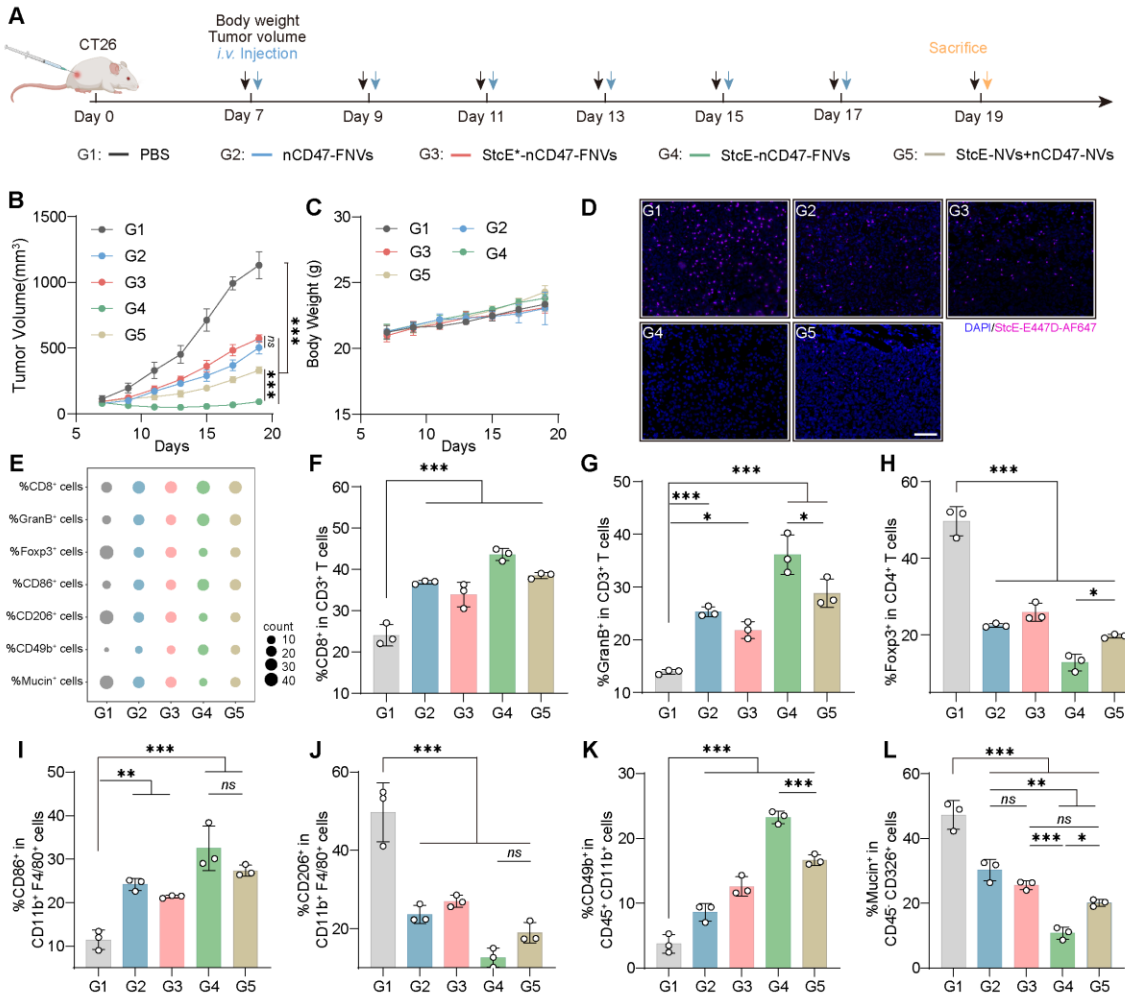

Fig. S30. *In vivo* antitumor efficacy of different treatments in CT26 tumor-bearing mice with expanded treatment groups. (*A*) Schematic timeline of the *in vivo* therapeutic experiment. (*B*) Tumor growth of CT26 tumor-bearing mice in each treatment group. (*C*) Body weight changes of mice in each treatment group. (*D*) Representative immunofluorescence images of Mucin$^+$ cells in tumors. Scale bar, 100μm. (*E*) Quantitative analysis of various immune cells. (*F*) Flow cytometry quantification of CD8$^+$ T cells in tumors. (*G*) Flow cytometry quantification of GranB$^+$ T cells in tumors. (*H*) Flow cytometry quantification of Foxp3$^+$ CD4$^+$ T cells in tumors. (*I*) Flow cytometry quantification of CD86$^+$ macrophages in tumors. (*J*) Flow cytometry quantification of CD206$^+$ macrophages in tumors. (*K*) Flow cytometry quantification of NK cells in tumors. (*L*) Flow cytometry quantification of Mucin$^+$ cells among CD45$^-$CD326$^+$ cells in tumors. Data are presented as mean ± S.D. (n = 4 for *B*-*C*. n = 3 for *D*-*L*). *P < 0.05, **P < 0.01, ***P < 0.001.

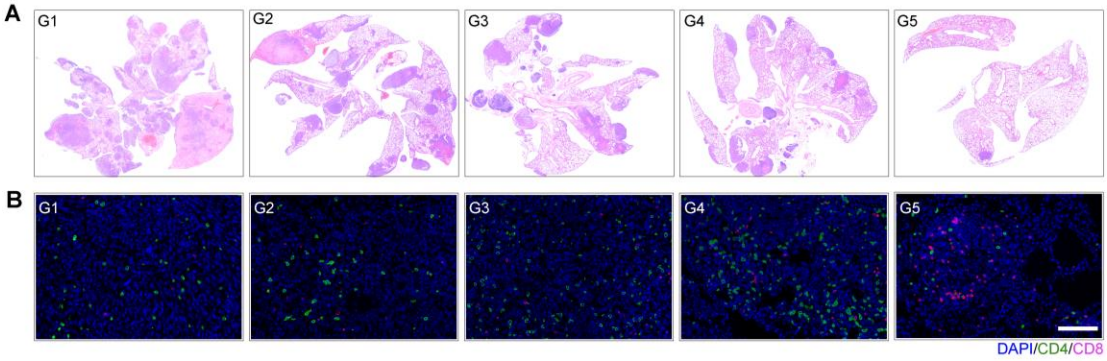

Fig. S31. Histological analysis of lung metastases after different treatments. (*A*) H&E-stained lung sections of different group. (*B*) Representative immunofluorescence images of infiltration of $CD8^+$ T cells (red) and $CD4^+$ T cells (green) in tumors. Scale bar, 100 μm. Related to Fig. 5.

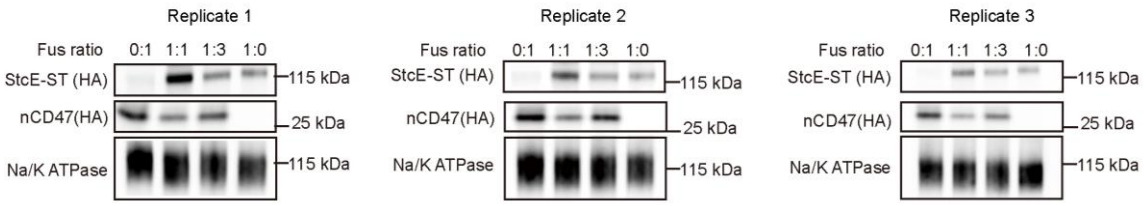

Fig. S32. Three replicates of Western blot analysis of nCD47 and StcE-ST in StcE-nCD47-FNVs.

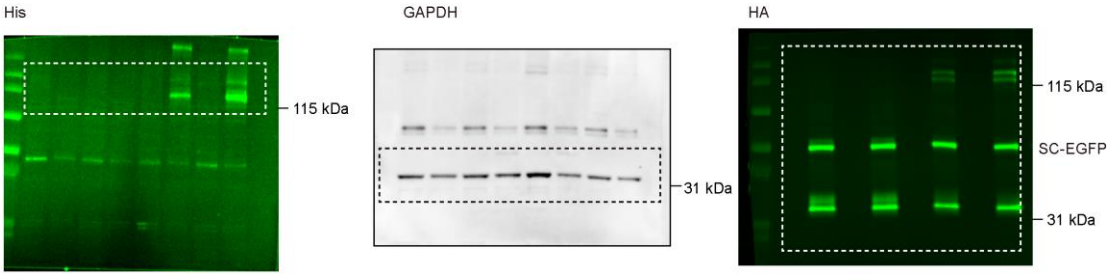

Fig. S33. Unprocessed Western blots for Fig. 1E. All the IR fluorescence western blots were converted into grayscale images by Fiji imageJ.

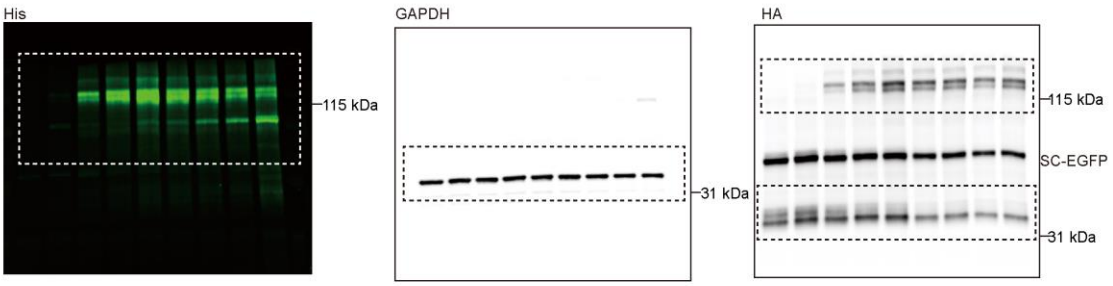

Fig. S34. Unprocessed Western blots for Fig. 1G. All the IR fluorescence western blots were converted into grayscale images by Fiji imageJ.

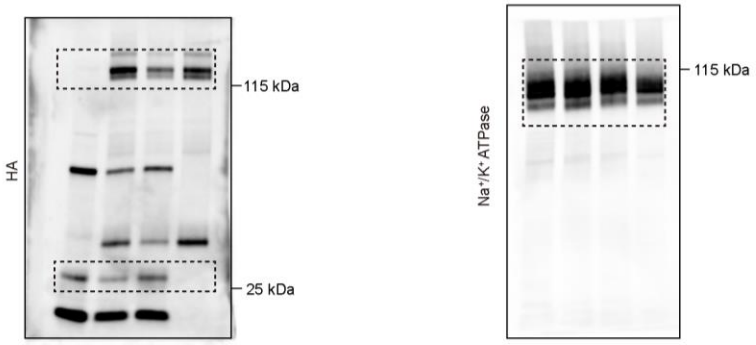

Fig. S35. Unprocessed Western blots for Fig. 2J.

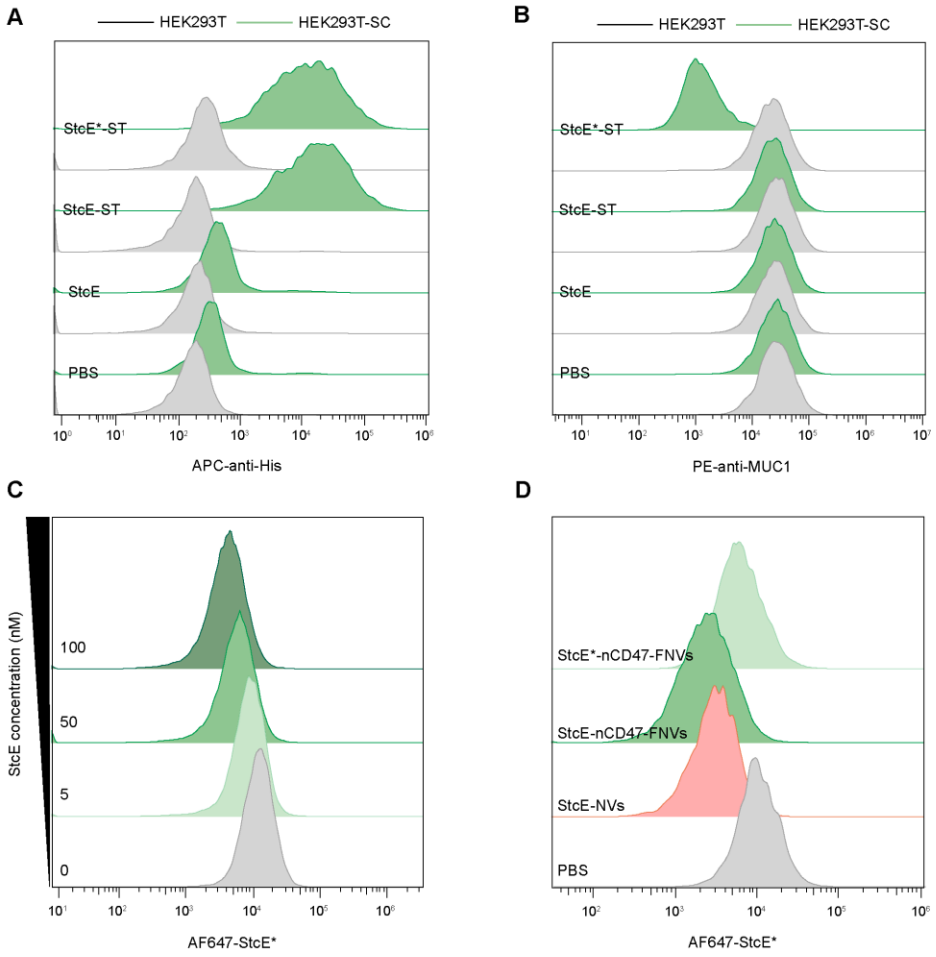

Fig. S36. The raw flow cytometry plots. (*A*) The raw flow plot of Fig. 1F. (*B*) The raw flow plot of Fig. 2B. (*C*) The raw flow plot of Fig. 2C. (*D*) The raw flow plot of Fig. 2N.